

Visualizing Invisible Dark Matter Annihilation with the CMB and Matter Power Spectrum

Yanou Cui^{1,*} and Ran Huo^{1,†}

¹*Department of Physics and Astronomy, University of California, Riverside, California 92521, USA*

(Dated: May 17, 2018)

We study the cosmological signatures of Invisibly Annihilating Dark Matter (IAnDM) where DM annihilates into dark radiation particles that are decoupled from the Standard Model (SM). In a large class of dark sector models such invisible annihilation determines the relic abundance of DM via dark thermal freezeout. We demonstrate that IAnDM may reveal itself through observable, novel signatures that are correlated: scale-dependent ΔN_{eff} (number of extra effective neutrinos) in the Cosmic Microwave Background (CMB) spectrum due to DM residual annihilation, while the phase of acoustic peaks shift towards the opposite direction relative to that due to SM neutrinos, resembling the effect due to scattering (fluid-like) thermal dark radiation; in addition, IAnDM induces modifications to the matter power spectrum that resemble yet are distinct from that due to warm dark matter. Current data is sensitive to IAnDM with masses up to ~ 200 keV, while future observations will improve the reach, especially if the late-time DM annihilation cross-section is enhanced relative to the standard thermal value, which can be realized in a variety of scenarios.

I. Introduction

Over the past two decades, we have seen overwhelming gravitational evidence for the existence of dark matter (DM) which constitutes 80% of the total matter density in our universe today. Nevertheless, the non-gravitational, particle nature of DM remains mysterious. Among the many theoretical candidates for DM, the Weakly Interacting Massive Particle (WIMP) is a well-motivated scenario that has played a central role in guiding the experimental searches for DM. The key process in WIMP models is the annihilation of DM into Standard Model (SM) particles which determines the relic abundance of DM after its thermal freezeout in the early universe. The residual DM annihilation today is potentially observable through indirect detection experiments. More recently, it has been realized that cosmological observations, in particular, the Cosmic Microwave Background (CMB), may serve as another path for observing DM annihilation that is free of astrophysical uncertainties [1–3]. These CMB studies focus on the effects of *visible* SM states (e.g., e^\pm, γ) on the recombination history of the universe.

Recently, driven by the strengthening experimental constraints on WIMP DM, there has been a growing interest in dark sector scenarios, where DM resides in a hidden sector with multiple states and/or self-interactions, in analogy to the complex structure of the SM. In a large class of dark sector models, the merit of predicting DM relic abundance from thermal freezeout is retained, yet the DM predominantly annihilates into other dark states instead of SM particles [4–15]. By decoupling the thermal relic abundance from couplings to the SM, these models are relieved from conventional DM constraints, yet call for new strategies for detection. The most challenging case arises when DM undergoes *invisible annihilation*, i.e., when DM annihilates into stable dark radiation (DR) particles that are decoupled from the SM. Can we *directly* observe/constrain this apparent nightmare (yet minimal and generic) scenario of Invisibly Annihilating DM (IAnDM) with cosmological data? In this *Letter* we will demonstrate a positive answer to this question: while the thermal ΔN_{eff} of DR [13] in IAnDM can be significantly suppressed if the

dark sector is much colder than the SM, an observable yet *non-standard* ΔN_{eff} effect can result from the non-thermal DR directly produced from DM annihilation. For IAnDM to yield detectable gravitational effects in the CMB and matter power spectrum (MPS), DM needs to be light and copious. In such mass range, modifications to MPS is dominantly affected by (*cold*) DM free-streaming, yet is distinctive from a warm DM (WDM) MPS. IAnDM with masses under ~ 200 keV is disfavored by current data, while future experiments will improve the sensitivity reach, especially if the late-time annihilation cross-section is enhanced relative to the standard thermal value. Note that although IAnDM was originally motivated in the context of thermal DM, it can arise from broader classes of models where an enhanced cross-section can be generally realized (see discussion in Section. V).

II. An Example Model

The scenario of IAnDM can be generally realized in particle physics models with thermal DM or beyond, while our main results are largely model-independent. We consider a simple example model where SM singlet fermionic DM χ annihilates into lighter fermionic DR particle ψ through a vector current interaction (Z' mediator), with s -wave thermal cross section, $\langle\sigma v\rangle$, which determines the relic abundance of χ . The relevant Lagrangian is:

$$\mathcal{L} \supset i\bar{\chi}\not{D}\chi + i\bar{\psi}\not{D}\psi - m_\chi\bar{\chi}\chi - m_\psi\bar{\psi}\psi - \frac{1}{4}Z'_{\mu\nu}Z'^{\mu\nu} + \frac{1}{2}m_{Z'}^2Z'^2,$$

where D_μ is the covariant derivative including Z' gauge interaction. The automatic self-scattering of ψ mediated by a moderately massive Z' is generally ineffective at late times, so that ψ free-streams then. The alternative case where ψ efficiently scatters at late times is possible with additional interactions [13].

Without additional effective interactions between ψ and the SM or other dark states, χ and ψ freeze out simultaneously as $\bar{\chi}\chi \rightarrow \bar{\psi}\psi$ departs from equilibrium. If ψ is massive enough, its relic density today can dominate over that of χ [16], which is an interesting alternative scenario that we will leave for future investigation. In this work we will assume that χ is the leading DM and thus the prediction for DM relic density re-

sembles that of the standard WIMP DM. This would require ψ to be in form of dark radiation, much lighter than χ and freezes out while it is relativistic. The temperature of a decoupled dark sector (χ, ψ) can be much colder than the SM, depending on the reheating pattern [17, 18] and the number of heavier states that have decoupled in each sector. The temperatures of χ, ψ also redshift differently after their freezeout. For the interest of this work, the relevant effect can be simply parametrized by $\xi \equiv \frac{\hat{T}_f}{T_f}$ around the dark thermal freezeout, where \hat{T}_f is the dark temperature and T_f is the SM one [46].

The relic abundance of χ can be estimated as in [5, 13]. We define freezeout temperature parameters $x_f \equiv \frac{m_\chi}{T_f}$, $\hat{x}_f \equiv \frac{m_\chi}{\hat{T}_f} = \frac{x_f}{\xi}$. Assuming $\xi < 1$ and s-wave annihilation, we have

$$x_f \simeq \xi \ln \left(\sqrt{\frac{45}{16}} \frac{1}{\pi^3} \frac{g_\chi}{\sqrt{g_*}} m_\chi M_P \langle \sigma v \rangle \xi^{\frac{5}{2}} \right) \simeq \xi \hat{x}_f, \quad (1)$$

$$\begin{aligned} \Omega_\chi &\simeq \sqrt{\frac{45}{\pi}} \frac{s_0}{\rho_c M_P} \frac{\sqrt{g_*}}{g_{*s}} \frac{\xi \hat{x}_f}{\langle \sigma v \rangle} \\ &= 0.32 \left(\frac{\hat{x}_f}{10} \right) \left(\frac{\sqrt{g_*}}{\sqrt{3.38}} \frac{43/11}{g_{*s}} \right) \left(\frac{3 \times 10^{-26} \text{ cm}^3 \text{ s}^{-1}}{\langle \sigma v \rangle / \xi} \right), \end{aligned} \quad (2)$$

where M_P is the Planck mass, s_0 and ρ_c are today's entropy and critical density respectively, g_χ is the internal degree of freedom (d.o.f) of χ , g_* , g_{*s} are the total effective d.o.f.'s dominated by SM states. With Eq. 2 it is important to note that a fixed $\langle \sigma v \rangle / \xi \simeq \sigma_0 \equiv 3 \times 10^{-26} \text{ cm}^3 \text{ s}^{-1}$ is required to yield correct thermal DM abundance, therefore for $\xi < 1$, the required $\langle \sigma v \rangle$ is reduced by ξ accordingly. For a light sub-MeV DM, $\hat{x}_f \sim 10$ (smaller than x_f of a typical WIMP), and around the DM freezeout $g_* = 3.38$, $g_{*s} = 43/11$ (the SM values after neutrino decoupling). In order to make sure that ψ does not over close the Universe, or dominate over Ω_χ , we also check the thermal relic density of ψ . For a massive ψ that freezes out as a hot relic,

$$\Omega_{\psi, \text{th}} = \frac{m_\psi n_\psi}{\rho_c} = 0.038 \left(\frac{m_\psi}{1 \text{ eV}} \right) \hat{g}_\psi \xi^3; \quad (3)$$

in the limit of massless ψ ,

$$\Omega_{\psi, \text{th}} = 2.7 \times 10^{-4} \hat{g}_\psi \xi^4, \quad (4)$$

where the subscript ‘‘th’’ denotes the thermal relic component of ψ , which distinguishes itself from the non-thermal component from χ annihilation that we will focus on (denoted by subscript ‘‘nth’’). We see that by allowing the general possibility of a colder dark sector, a moderately massive ψ can be cosmologically viable. Note that for $\xi \ll 1$, $\Omega_{\psi, \text{th}}$ is strongly suppressed, easily making ψ a subleading component relative to χ .

III. Cosmological Effects of Invisible DM Annihilation: General Consideration and Analytic Studies

In this section we study potential cosmological effects of IAnDM with analytic approaches, with numerical results following in Section. IV.

The non-thermal free-streaming DR ψ injected from DM χ annihilation contributes an additional radiation-like energy component to the Universe. The accumulated energy density of ψ from χ annihilation, $\rho_{\psi, \text{nth}}$, can be estimated as follows. Assuming $m_\psi = 0$ for simplicity, a straightforward estimate based on energy conservation gives $d\rho_{\psi, \text{nth}}(\hat{t}) = \rho_\chi n_\chi \langle \sigma v \rangle d\hat{t}$. Upon integration over time with proper redshift factors, the accumulated ψ density by the time t (a) is:

$$\begin{aligned} \rho_{\psi, \text{nth}}(a) &= \frac{\rho_c^2 \Omega_\chi^2}{m_\chi} \int_{a_i}^a \frac{1}{\tilde{a}^6} \langle \sigma v \rangle \frac{\tilde{a} d\tilde{a}}{H_0 \sqrt{\Omega_{\gamma+\nu}}} \left(\frac{\tilde{a}}{a} \right)^4 \\ &= \left(\frac{3H_0^2 \Omega_\chi}{8\pi G} \right)^2 \frac{\langle \sigma v \rangle}{m_\chi H_0 \sqrt{\Omega_{\gamma+\nu}}} \frac{\ln(\frac{a}{a_i})}{a^4}, \end{aligned} \quad (5)$$

where deep radiation dominated (RD) epoch is assumed to show a neat analytic form, and we have used the convention that current day $a_0 = 1$. a_i represents the initial time when the net ψ production from χ annihilation becomes effective which is around the freezeout time, $a/a_i \sim T_f/T$. Note that in addition to the standard redshift $1/a^4$, there is a moderate *log-dependence* on a which is absent in the energy density of a standard thermal radiation background.

In order to relate to the potential CMB observable, ΔN_{eff} , we take the ratio of $\rho_{\psi, \text{nth}}$ over SM neutrino density (one flavor), and find

$$\Delta N_{\text{eff, nth}}(a) = 0.038 \ln \left(\frac{a}{a_i} \right) \left(\frac{\text{keV}}{m_\chi / \xi} \right) \left(\frac{\langle \sigma v \rangle / \xi}{3 \times 10^{-26} \text{ cm}^3 / \text{s}} \right), \quad (6)$$

where $a \approx 10^{-3}$ when evaluated around the CMB epoch. Note that $\Delta N_{\text{eff, nth}}$ inherits the aforementioned $\ln(a/a_i)$ dependence. Apparently lighter DM produce more copious ψ and thus more pronounced signals. We can also see that with $\xi = 1$ and thus $\langle \sigma v \rangle$ taking the standard thermal value σ_0 , an $O(1) - O(10)$ keV mass χ could lead to observable ΔN_{eff} at current or upcoming CMB experiments [19–21], while for $\xi < 1$ and fixed $\langle \sigma v \rangle / \xi \equiv \sigma_0$ a lighter χ is required to yield the same ΔN_{eff} . To account for this ξ dependence, in Fig.1 and later figures we parametrize with the rescaled DM mass, m_χ / ξ .

If $m_\psi \lesssim \text{eV}$, there would be another irreducible contribution to ΔN_{eff} from the thermal relic of ψ (Eq. 4):

$$\Delta N_{\text{eff, th}} = 3.046 \frac{\rho_{\psi, \text{th}}}{\rho_\nu, 1} = \frac{4}{7} \left(\frac{11}{4} \right)^{\frac{4}{3}} \hat{g}_\psi \xi^4 = 2.2 \hat{g}_\psi \xi^4. \quad (7)$$

Comparing this with the $\Delta N_{\text{eff, nth}}$ given in Eq. 6, we can see that the novel, non-thermal contribution easily dominates for small ξ , which will be the focus of this work. Fig. 1 illustrates the physics discussed above. In the upper panel we plot the deviation of the DM's co-moving density, Y_χ , from its value of today (due to residual annihilation into ψ) as a function of a . Y_χ is calculated by numerically solving the Boltzmann equation around DM freezeout ($m_\psi = 0$, including proper redshift for both RD and matter-dominated (MD) eras). In the lower panel we plot the evolution of the resulting $\Delta N_{\text{eff, nth}}$, as well as the thermal component $\Delta N_{\text{eff, th}}$ (Eq. 7)

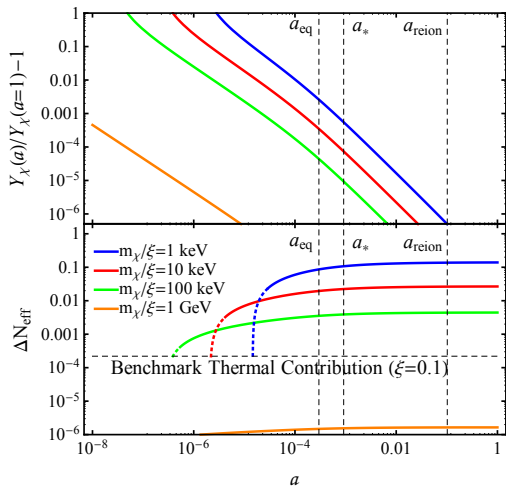


FIG. 1: Upper panel: the slow depletion of Y_χ due to its residual annihilation. Lower panel: ΔN_{eff} due to massless annihilation product ψ . a_{eq} , a_* , a_{reion} are the expansion parameters, at the matter-radiation equality, recombination and reionization epochs, respectively.

with a benchmark value $\xi = 0.1$. Apparently the residual annihilation induced $\Delta N_{\text{eff, nth}}$ can be sizable for sufficiently light DM χ , and easily dominates over $\Delta N_{\text{eff, th}}$.

IAnDM model may also affect MPS in various ways. For the parameter range that leads to observable effects (light χ), numerical results (Sec. IV) show that the dominating factor is the free-streaming of χ following its freezeout. This effect is *novel* and may seem counter-intuitive as free-streaming is often related to hot or warm relics. Here although IAnDM freezes out as a cold relic, with sufficiently small mass (e.g. $O(100)$ keV), it decouples late enough to sustain a non-negligible free-streaming effect at structure formation time. As shown in the later Fig. 3, at leading order the MPS from an IAnDM model with m_χ/ξ resembles that due to a WDM model with a corresponding m_{WDM} . The $\chi - \psi$ scattering, if in equilibrium, may induce a competing suppression through dark acoustic oscillation, but we have checked that with a massive Z' ($m_{Z'} > m_\chi$) the $\chi - \psi$ kinetic decoupling occurs early enough and does not affect MPS effectively [22]. Here we demonstrate analytically the correspondence between IAnDM and WDM by matching the free-streaming velocity, $v_{\text{FS}}(a)$, in the two models, which appears in perturbation Boltzmann equations [23] and determines transfer functions. This is similar to deriving analogous correspondence between the sterile neutrino case and WDM [24]. In non-relativistic limit, $v_{\text{FS}}(a) = \frac{\tilde{p}}{E} \rightarrow \frac{\tilde{p}}{m} \frac{1}{a}$, where $\tilde{\cdot}$ denotes co-moving quantities. Therefore if the v_{FS} 's match today ($a = 1$), they also match at earlier times relevant to structure formation. Taking into account the specifics around freezeout time for IAnDM and WDM models, we find that at $a = 1$: $\tilde{p}_{\text{WDM}} = \left(\frac{2\pi^2}{3\zeta(3)} \frac{\rho_{\text{WDM}}}{m_{\text{WDM}}} \right)^{\frac{1}{3}}$, $\tilde{p}_\chi = \sqrt{2\hat{x}_f} \xi T_\gamma$, where T_γ is T_{CMB} today. Equating $\frac{\tilde{p}}{m}$ in the

two models, we find the correspondence:

$$m_{\text{WDM}} = \left(\frac{2\pi^2 \rho_{\text{WDM}}}{3\zeta(3)} \right)^{\frac{1}{4}} \left(\frac{m_\chi/\xi}{T_\gamma \sqrt{2\hat{x}_f}} \right)^{\frac{3}{4}} = 0.08 \left(\frac{m_\chi/\xi}{\text{keV}} \right)^{\frac{3}{4}} \text{ keV}, \quad (8)$$

where we took $\rho_{\text{WDM}} = \rho_{\text{DM},0}$, $x_f = 10$.

IV. Numerical Studies

In order to relate to observations in a more precise way, we further perform a numerical analysis by solving the perturbation Boltzmann equations for the evolution of the χ, ψ system using `camb` [25]. The general formulation follows [23] with the choice of synchronous gauge. The dominant DM, χ , follows the standard treatment while allowing DM free-streaming effect, and the annihilation term can have a non-negligible impact on its evolution. The initial perturbation of the annihilation product, ψ , inherits that of χ (CDM), while its later evolution follows the same perturbation multipole expansion as the massless or massive neutrinos. However there are key differences between neutrinos and the ψ produced from DM annihilation. First, unlike neutrinos, the unperturbed partition function $f(\tilde{p})$ of ψ is not thermal, rather it is given by the annihilation process with a fixed physical momentum (determined by m_χ, m_ψ). The $f(\tilde{p})$ feeds into the perturbation equations through the factor of $\frac{\partial \ln f(\tilde{p})}{\partial \ln \tilde{p}}$, which can be replaced by -4 for massless neutrinos. For our non-thermally produced ψ , this factor can be calculated in the same way as in [26], which at leading order yields: $\frac{\partial \ln f(\tilde{p})}{\partial \ln \tilde{p}} = -\frac{9}{2} + \frac{3\tilde{p}}{2\bar{p}}$, where \tilde{p}, \bar{p} are the background pressure and energy density. Deep in RD regime $\tilde{p} = \frac{1}{3}\bar{p}$, $\frac{\partial \ln f(\tilde{p})}{\partial \ln \tilde{p}}$ coincidentally gives -4 . Numerically we also include a small correction to this factor on the order of $O(\frac{\Gamma_{\text{ann}}}{H})$. In addition, the annihilation product will slightly change the equation of state, thus changing the Hubble expansion rate, H , which we take into account numerically. Beyond these differences, the contribution from annihilation products to the Boltzmann equations are coded in parallel to massless or massive neutrinos. We modify `camb` [25] to incorporate these new physics considerations, and choose the standard cosmology parameters: $h = 0.678$, $\Omega_\chi h^2 \approx \Omega_{\text{DM}} h^2 = 0.1186$, $\Omega_b h^2 = 0.02226$, etc. [20]

Numerical Results: The CMB Signatures

In order to demonstrate the effects of ψ produced from invisible DM annihilation in a visible and representative way, in Fig. 2 we plot the zoomed-in CMB TT spectra around the first and the sixth acoustic peaks, for a set of m_χ/ξ choices. We assume $m_\psi = 0$ which represents the general case of $m_\chi \gg m_\psi$ that we focus on. For comparison we also plot the spectra based on CDM and models with extra neutrinos for a set of ΔN_{eff} values. As expected based on our analytic estimate (Eq.6), the effects from ψ injection at leading order resemble that from standard ΔN_{eff} , which as shown below are confirmed by numerical studies. However, there are key differences between a genuine ΔN_{eff} and the ΔN_{eff} -like effect caused by non-thermal ψ , which we will also explain as follows. These novel, distinct effects induced by IAnDM can be detectable with high precision CMB observation and dedi-

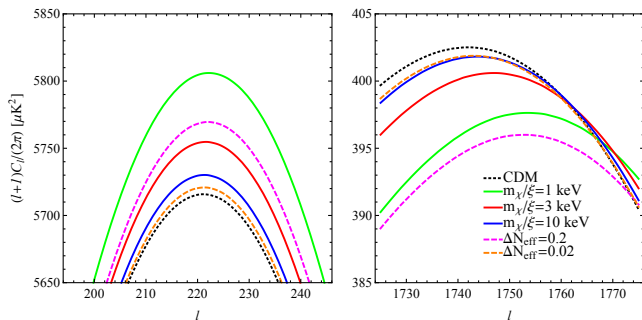


FIG. 2: Left panel: CMB TT mode around the first acoustic peak. Right panel: around the sixth acoustic peak. Also shown are the CDM and $\Delta N_{\text{eff}} = 0.02, 0.2$ spectra for comparison.

cated analyses.

The most notable effect on the CMB spectrum due to ΔN_{eff} or non-thermal ψ in IAnDM is on the heights of the acoustic peaks. In both models, the change to H due to additional radiation energy density leads to the increase in the height of the first peak (i.e., early integrated Sachs-Wolfe (ISW) effect), and the decrease in that of the higher peaks (i.e., enhanced Silk damping). However, the heights of CMB acoustic peaks from IAnDM do not align with those due to a fixed standard ΔN_{eff} . As expected based on Eq. 6 and Fig. 1, $\Delta N_{\text{eff,ntth}}$ varies over time as $\rho_{\psi,\text{ntth}}$ accumulates while χ continues to annihilate. This can be seen by comparing the amplitudes of the CMB spectrum shown in Fig.2 where higher ℓ corresponds to an earlier time (when the mode re-enters horizon): consider a fixed $m_\chi/\xi = 1$ keV, around the 6th peak the resulting CMB TT spectrum roughly aligns with that associated with $\Delta N_{\text{eff}} \approx 0.12$; while around the 1st peak, it aligns with a larger $\Delta N_{\text{eff}} \approx 0.35$.

The standard ΔN_{eff} also reveals itself via a unique phase shift of the high ℓ acoustic peaks due to neutrino-like modes that induce a significant anisotropic stress and propagate faster than the sound speed (free-streaming) [27, 28], which cannot be caused by other standard physics [47]. IAnDM induces a phase shift as well, yet with dramatic difference compared to that caused by standard ΔN_{eff} . We found that by adjusting h , $\Omega_{\text{DM}} h^2$, Y_{He} to match the CMB observables of θ_* , θ_D and z_{eq} [20], in the IAnDM model the locations of the acoustic peaks shift towards high ℓ 's, *opposite* to the direction expected from standard free-streaming ΔN_{eff} [27]. (We found that due to the presence of non-thermal DR, the best fit of h shifts to higher values, which helps alleviate the discrepancy in H_0 measurements between the CMB observation and local measurements). Such an effect resembles that due to a fluid-like or scattering DR species [13, 28, 29], yet for different reasons. Even though free-streaming, unlike neutrinos, the non-thermal ψ dominantly produced at late times inherits a negligible initial anisotropic stress from χ , and consequently would not induce an additional phase shift along the same direction as neutrinos [48]. However, such ψ does contribute to late-time radiation energy density, and thus reduce the energy

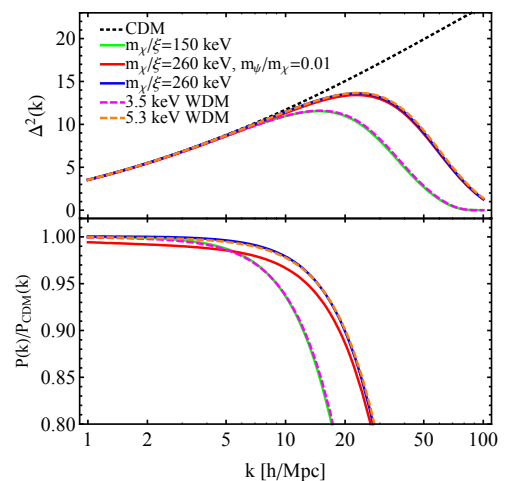


FIG. 3: Matter power spectra for different DM χ masses and different m_ψ/m_χ and $\langle\sigma v\rangle$ ($m_\psi = 0$, with one exception). Also shown are the 3.5 keV, 5.3 keV WDM spectra (sitting on the current conservative and aggressive Lyman- α bound).

fraction of the free-streaming SM neutrinos. As noted in [13] a reduction of free-streaming neutrinos fraction (due to fluid-like DR or non-thermal ψ here) leads to a phase shift along the direction opposite to that due to standard ΔN_{eff} . Furthermore, just as with peak heights, there is scale dependence in phase shifts, which is a higher order effect that may distinguish IAnDM from fluid-like DR. [49]

Numerical Results: The Matter Power Spectra

In Fig. 3 we present the MPS in the scenario of IAnDM, in comparison with other familiar new physics scenario: CDM, and WDM with masses saturating current conservative and aggressive Lyman- α bound [30]. The definition of matter power spectra $P(k)$, $\Delta^2(k)$ are standard, e.g., as given in [31]. Compared to the standard CDM prediction, all these new models cause a suppression of MPS relative to the standard cosmology for $k \gtrsim 1$ h/Mpc. The upper panel $\Delta^2(k)$ shows that the IAnDM spectra well overlaps with WDM spectra with a corresponding mass estimated by Eq. 8. This implies that the χ free-streaming is the dominant effect determining MPS due to IAnDM. Nevertheless, the zoomed-in bottom panel of Fig. 3 shows slight differences between IAnDM and WDM spectra. We demonstrate such differences with $m_\chi/\xi = 260$ keV, allowing a massive ψ (still require $m_\psi \ll m_\chi$ to be consistent with our starting assumption on cosmology). Here we see that the suppression on small scales is more pronounced for a massive ψ . This can be understood as the energetic ψ produced by χ annihilation eventually clusters as a component of DM and leads to a secondary free-streaming effect.

V. Summary and Discussion

With our understanding of the IAnDM effects on the CMB and the MPS, we can derive constraints based on current data and project sensitivities for future experiments. An optimized precision calculation for this purpose requires a large sam-

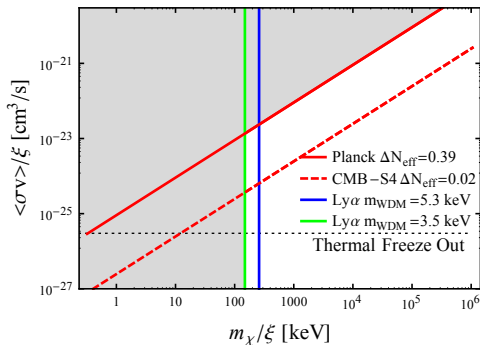


FIG. 4: The constraints on invisible DM annihilation from Planck and Lyman- α measurements and the sensitivity forecast for CMB-S4 ($m_\psi = 0$, shaded region is excluded). The axes are labeled by taking into account the rescaling factor $\xi = T_{\text{DM}}/T_{\text{SM}}$ at freezeout time.

pling of the annihilation product’s comoving momentum [50] and is beyond the scope of the current *Letter*. Thus we will not derive the rigorous global constraints by the standard MCMC method, rather will simply recast the current constraints by comparing physical effects analytically.

The results are summarized in Fig. 4, where we label the axes with the scaling factor ξ to account for the generic colder dark sector possibility. The CMB constraint is estimated by comparing the (projected) experimental sensitivity limit on ΔN_{eff} to our analytical formula Eq. 6. The above numerical studies suggests subtle differences from this estimate based on fixed ΔN_{eff} , while as aforementioned a rigorous constraint is beyond the scope of this work. On the other hand, the constraint from MPS can be extracted by comparing the DM free-streaming effect based on our Eq. 8. Note that the main effect of IAnDM on the CMB depends on the ratio $\langle\sigma v\rangle/m_\chi$ (Eq. 6). Assuming the thermal freeze-out annihilation cross section, the current 2σ bound from Planck (combined with BAO data) $\Delta N_{\text{eff}} \lesssim 0.39$ [20, 29] (here we used the bound on N_{tot} in [29], including both fluid-like and free-streaming dark radiation) can be recast into a bound of $m_\chi/\xi \gtrsim 0.3$ keV for $m_\psi \ll m_\chi$. In contrast, the main effect of IAnDM on MPS only depends on m_χ/ξ (Eq. 8), insensitive to $\langle\sigma v\rangle$. The current Lyman- α observation constrains IAnDM MPS: the 2σ aggressive bound ($m \gtrsim 5.3$ keV for WDM) corresponds to a bound of $m_\chi/\xi \gtrsim 260$ keV, and the conservative bound ($m \gtrsim 3.5$ keV for WDM) corresponds to a bound of $m_\chi/\xi \gtrsim 150$ keV. For a massive ψ the constraint from Lyman- α would be stronger due to additional free-streaming suppression as discussed in Sec. IV.

According to Fig. 4, Lyman- α disfavors IAnDM with $m_\chi/\xi \lesssim 150$ keV regardless of $\langle\sigma v\rangle$, while for larger masses CMB observations have sensitivities if the DM late-time annihilation cross-section is enhanced relative to the standard thermal value. Note that although in this work we considered a particular thermal IAnDM model as a simple example, the inferred novel phenomenology and the sensitivity plot

Fig. 4 apply to broader possibilities of IAnDM models allowing *enhanced annihilation cross-section* relative to the thermal value. Such possibilities have been well considered in the context of the familiar visibly annihilating DM, which generally apply for IAnDM, including: Sommerfeld enhancement [32, 33] (automatic in IAnDM if DR is a light mediator instead of a fermion), enhancement due to non-standard cosmology or non-thermal production of DM [34–36]. Phenomenological details of these variations require dedicated studies for specific models.

If the sensitivity of the future CMB-S4 experiment can be improved to $\Delta N_{\text{eff}} \simeq 0.02$ [21, 37–39], then the CMB sensitivity to thermal IAnDM can be improved to $m_\chi/\xi \gtrsim 10$ keV. So far Lyman- α forest observation provides the best probe for MPS relevant for IAnDM, with potential improvement by future 21 cm-line experiments [40]. With the presence of additional interactions beyond our minimal model, an effective DM-DR scattering may induce a more notable effect on large scale structure (σ_8) [14, 41, 42].

Astrophysical/cosmological observation is stepping into a high precision era, which enables us to probe well-motivated DM models that are beyond the reach of conventional DM detections. In this *Letter* we demonstrate a representative example by investigating the novel phenomenology from the generic scenario of Invisibly Annihilating DM (IAnDM). The smoking gun signature of this large class of models includes a correlated combination of scale-dependent, fluid-like ΔN_{eff} in the CMB spectra and a unique pattern of matter power spectrum that resembles WDM. The current data constrains the IAnDM with masses up to ~ 200 keV, while future experiments can be sensitive to larger masses if the DM annihilation cross-section is enhanced relative to the standard thermal value. These findings motivate new dedicated analyses to optimize the potential for discovering DM residing in a hidden sector.

Acknowledgments:

We thank Simeon Bird, Raphael Flauger, Takemichi Okui, Zhen Pan, Yuhsin Tsai and Hai-Bo Yu for discussion.

* Electronic address: yanou.cui@ucr.edu

† Electronic address: huora@ucr.edu

- [1] N. Padmanabhan and D. P. Finkbeiner, Phys. Rev. **D72**, 023508 (2005), astro-ph/0503486.
- [2] M. S. Madhavacheril, N. Sehgal, and T. R. Slatyer, Phys. Rev. **D89**, 103508 (2014), 1310.3815.
- [3] D. Green, P. D. Meerburg, and J. Meyers (2018), 1804.01055.
- [4] M. Pospelov, A. Ritz, and M. B. Voloshin, Phys. Lett. **B662**, 53 (2008), 0711.4866.
- [5] J. L. Feng, H. Tu, and H.-B. Yu, JCAP **0810**, 043 (2008), 0808.2318.
- [6] C. Cheung, G. Elor, L. J. Hall, and P. Kumar, JHEP **03**, 085 (2011), 1010.0024.

- [7] J. M. Cline and A. R. Frey, Phys. Lett. **B706**, 384 (2012), 1109.4639.
- [8] G. Belanger and J.-C. Park, JCAP **1203**, 038 (2012), 1112.4491.
- [9] M. Blennow, E. Fernandez-Martinez, O. Mena, J. Redondo, and P. Serra, JCAP **1207**, 022 (2012), 1203.5803.
- [10] C. Garcia-Cely, A. Ibarra, and E. Molinaro, JCAP **1402**, 032 (2014), 1312.3578.
- [11] K. Agashe, Y. Cui, L. Necib, and J. Thaler, JCAP **1410**, 062 (2014), 1405.7370.
- [12] J. Berger, Y. Cui, and Y. Zhao, JCAP **1502**, 005 (2015), 1410.2246.
- [13] Z. Chacko, Y. Cui, S. Hong, and T. Okui, Phys. Rev. **D92**, 055033 (2015), 1505.04192.
- [14] Z. Chacko, Y. Cui, S. Hong, T. Okui, and Y. Tsai, JHEP **12**, 108 (2016), 1609.03569.
- [15] M. H. Chan, Astropart. Phys. **80**, 1 (2016), 1604.01494.
- [16] M. Farina, D. Pappadopulo, J. T. Ruderman, and G. Trevisan, JHEP **12**, 039 (2016), 1607.03108.
- [17] Z. G. Berezhiani, A. D. Dolgov, and R. N. Mohapatra, Phys. Lett. **B375**, 26 (1996), hep-ph/9511221.
- [18] P. Adshhead, Y. Cui, and J. Shelton, JHEP **06**, 016 (2016), 1604.02458.
- [19] A. Suzuki et al. (POLARBEAR), J. Low. Temp. Phys. **184**, 805 (2016), 1512.07299.
- [20] P. A. R. Ade et al. (Planck) (2015), 1502.01589.
- [21] K. N. Abazajian et al. (CMB-S4) (2016), 1610.02743.
- [22] R. Huo, M. Kaplinghat, Z. Pan, and H.-B. Yu (2017), 1709.09717.
- [23] C.-P. Ma and E. Bertschinger, Astrophys. J. **455**, 7 (1995), astro-ph/9506072.
- [24] M. Viel, J. Lesgourgues, M. G. Haehnelt, S. Matarrese, and A. Riotto, Phys. Rev. **D71**, 063534 (2005), astro-ph/0501562.
- [25] A. Lewis, A. Challinor, and A. Lasenby, Astrophys. J. **538**, 473 (2000), astro-ph/9911177.
- [26] R. Huo, Phys. Lett. **B701**, 530 (2011), 1104.4094.
- [27] S. Bashinsky and U. Seljak, Phys. Rev. **D69**, 083002 (2004), astro-ph/0310198.
- [28] D. Baumann, D. Green, J. Meyers, and B. Wallisch, JCAP **1601**, 007 (2016), 1508.06342.
- [29] C. Brust, Y. Cui, and K. Sigurdson, JCAP **1708**, 020 (2017), 1703.10732.
- [30] V. Irsic et al., Phys. Rev. **D96**, 023522 (2017), 1702.01764.
- [31] S. Dodelson, *Modern Cosmology* (Academic Press, Amsterdam, 2003), ISBN 9780122191411.
- [32] N. Arkani-Hamed, D. P. Finkbeiner, T. R. Slatyer, and N. Weiner, Phys. Rev. **D79**, 015014 (2009), 0810.0713.
- [33] J. L. Feng, M. Kaplinghat, and H.-B. Yu, Phys. Rev. **D82**, 083525 (2010), 1005.4678.
- [34] G. B. Gelmini and P. Gondolo, Phys. Rev. **D74**, 023510 (2006), hep-ph/0602230.
- [35] J. Fan, O. zsoy, and S. Watson, Phys. Rev. **D90**, 043536 (2014), 1405.7373.
- [36] A. L. Erickcek, Phys. Rev. **D92**, 103505 (2015), 1504.03335.
- [37] W. L. K. Wu, J. Errard, C. Dvorkin, C. L. Kuo, A. T. Lee, P. McDonald, A. Slosar, and O. Zahn, Astrophys. J. **788**, 138 (2014), 1402.4108.
- [38] J. Errard, S. M. Feeney, H. V. Peiris, and A. H. Jaffe (2015), 1509.06770.
- [39] K. N. Abazajian et al. (Topical Conveners: K.N. Abazajian, J.E. Carlstrom, A.T. Lee), Astropart. Phys. **63**, 66 (2015), 1309.5383.
- [40] J. R. Pritchard and A. Loeb, Rept. Prog. Phys. **75**, 086901 (2012), 1109.6012.
- [41] M. A. Buen-Abad, G. Marques-Tavares, and M. Schmaltz, Phys. Rev. **D92**, 023531 (2015), 1505.03542.
- [42] J. Lesgourgues, G. Marques-Tavares, and M. Schmaltz, JCAP **1602**, 037 (2016), 1507.04351.
- [43] B. Follin, L. Knox, M. Millea, and Z. Pan, Phys. Rev. Lett. **115**, 091301 (2015), 1503.07863.
- [44] B. Audren, J. Lesgourgues, G. Mangano, P. D. Serpico, and T. Tram, JCAP **1412**, 028 (2014), 1407.2418.
- [45] V. Poulin, P. D. Serpico, and J. Lesgourgues, JCAP **1608**, 036 (2016), 1606.02073.
- [46] ξ is the same as r variable defined in [13].
- [47] Such an effect from SM neutrinos was recently detected with Planck data [43].
- [48] Although ψ may develop a larger anisotropic stress after production, our numerical analysis shows that its effect on CMB phase shift is subdominant to what we discussed in this paper.
- [49] Qualitatively the novel effects on CMB anisotropy spectrum we discussed here may also originate from the scenario of DM decaying to DR [26, 44, 45]. However, for decaying DM with long enough lifetime to be cosmologically stable and satisfy existing constraints, the amount of DR produced during CMB epoch is tiny and the resultant signal strength is expected to be negligible.
- [50] We use 50 (for MPS) to 500 (for CMB) discretized comoving momentum, while `camb` optimize to 3 to 5 for massive neutrino unless an extra accuracy boost is used.